



Tribological effects of micromilling of hardened AISI D2 steel on tool wear and top burr formation

Anderson Júnior dos Santos^{1,2} · Bárbara Cristina Mendanha Reis³ · Natália Fernanda Santos Pereira⁴ · Diogo Azevedo de Oliveira¹ · Juan Carlos Campos Rubio¹ · Alexandre Mendes Abrão¹ · Marcelo Araújo Câmara¹

Received: 28 February 2023 / Accepted: 19 June 2023 / Published online: 12 July 2023
© The Author(s), under exclusive licence to Springer-Verlag London Ltd., part of Springer Nature 2023

Abstract

The study of micromilling of quenched and tempered AISI D2 steel is of utmost importance due to the accelerated wear of the micromilling cutting tool edge that intensifies the formation of top burrs, which is detrimental to the micromilled surfaces because it requires further surface finishing. In this work, the effect of tooth feed per tooth and axial depth of cut on machining forces and top burr formation after dry micromilling of slots in quenched and tempered AISI D2 steel was evaluated. The results show that the passive force is approximately 32% higher than the radial and feed forces. Regarding burr formation, axial depth of cut was the most relevant parameter. Doubling axial depth of cut burr height increased by approximately 400%. Increasing feed per tooth reduces burr formation. The down cutting direction presented top burr heights approximately 23% higher when compared with up cutting. Attrition was the predominant tool wear mechanisms. Tool wear increases progressively with machining length raising the micromilling force components, which leads to rounding and increasing the radius of the cutting edge. Consequently, a negative rake angle is generated, inducing size effect and intensifying the material plowing mechanism.

Keywords Micromilling · Hardened AISI D2 steel · Micromilling forces · Roughness · Wear mechanisms

1 Introduction

The technological development of some industrial sectors drives the increasing demand for compact and integrated products in the form of miniatures, such as electronics, heat exchangers, sensors, and actuators [1–4]. In the production

of microcomponents, the use of micro-dies is widespread, with micromilling being the most commonly used technique, along with the use of coated tungsten carbide micro-endmills and AISI D2 steel being the main work materials employed [5]. Micromilling is a relevant technique for producing micro-dies and machining of die corners, as larger end mills cannot operate in these areas due to their limited capacity to work with small dimensions. With higher precision and control, micro-endmills have the ability to reach narrow corners and produce high-quality finishes [6].

Micromilling is justified in machining corners of D2 steel dies where larger end mills cannot perform milling due to their ability to machine components with reduced dimensions and intricate details. With greater precision and control, micro-endmills can access narrow corners and produce high-quality finishes.

AISI D2 tool steel belongs to group D for cold working. This material is commonly subjected to quenching and tempering, thus resulting in a microstructure composed of martensite, retained austenite, and carbides, which ensures high hardness and wear resistance which is attributed to the presence of chromium carbides in the microstructure of the

✉ Anderson Júnior dos Santos
andersonsantoscefet@gmail.com;
andersonsantos@cefetmg.br

¹ Mechanical Engineering Graduate Program, Universidade Federal de Minas Gerais, Av. Antônio Carlos, 6627. Campus Pampulha, Belo Horizonte, Minas Gerais 31270-901, Brazil

² Department of Materials Engineering, Federal Center for Technological Education of Minas Gerais, Av. Amazonas, 5253, Nova Suiça, Belo Horizonte, Minas Gerais 30421-169, Brazil

³ Department of Urban Engineering, Federal University of Ouro Preto, University Campus of Morro Do Cruzeiro, S/N, Ouro Preto, Minas Gerais 35400-000, Brazil

⁴ Industrial Engineering Graduate Program, Universidade Federal de Minas Gerais, Av. Antônio Carlos, 6627. Campus Pampulha, Belo Horizonte, Minas Gerais 31270-901, Brazil

material [7]. For these reasons, this material is widely used for the production of dies and molds [8, 9]. In this context, machining hardened AISI D2 steel can lead to severe wear of the cutting tool and to its premature fracture.

The most important aspect that characterizes micromachining is the size effect that influences the cutting mechanisms and changes the micromilling forces, machined surface roughness, and the energy consumed during chip and burr formation. Burr formation in micromilling is inevitable, and the causes are commonly related to the cutting tool geometry, cutting speed, feed per tooth, axial depth of cut, and workpiece material [10, 11]. In addition to that, dynamic factors such as cutting tool wear, vibration, tool eccentricity, temperature variation, and the effect of applying fluids with cooling/lubricating action also contribute to changes in burr formation [12]. Generally, burrs are removed after machining. However, their removal cannot always be performed due to accuracy requirements for the microcomponent, since deburring can induce residual stresses and dimensional changes that affect its functionality [9]. Therefore, strategies must be devised during micromilling to reduce burr formation. This approach is more suitable in terms of machining costs and time.

To determine the best strategy to be adopted, substantial knowledge regarding the influence of cutting parameters on micromilling and the metallurgical nature of the material is required, since burr formation is strongly influenced by these factors. Bajpai et al. [13] and Biermann et al. [14] noted that micromilling performed at lower feed per tooth leads to increased burr height due to the smaller ratio of the tool edge radius to the undeformed chip thickness, which intensifies the plowing mechanism. The authors also stated that burr formation during micromilling can be in terms of ductility, crystallographic orientation, and grain size of the work material. Bajpai et al. [3] and Chen et al. [15] stated that the axial depth of cut was the only parameter that significantly affected burr width and that the burr volume formed during up micromilling is usually smaller than that formed when down micromilling.

In micromilling, it is usual to monitor tool wear through direct or indirect measurement techniques. Direct methods involve obtaining specific variable values directly and observing dimensional changes in the tool and/or workpiece [16]. In the context of micromilling, scanning electron microscopy (SEM) is widely used to identify visual signs of wear, such as flank wear, cutting edge wear, and burr formation. Additionally, SEM allows for the verification of tool dimensions, such as length, diameter, and angles, to identify wear-induced alterations [17]. On the other hand, indirect methods rely on empirical relationships, such as machining force, noise generated during micromilling operations, vibration, temperature, and acoustic emission signals, to determine the actual tool wear [18]. Profilometry

is a technique employed to measure machined surface roughness and the presence of burrs resulting from micromilling, providing indirect indications of wear [19].

For the proper selection of micromilling parameters that minimize burr formation and result in better product quality, it is of utmost importance to understand the tribological effects of micromilling that lead to intrinsic wear of the cutting edge and, mainly, the relationship between wear mechanisms and burr formation. Burr dimensions increase as tool wear progresses [20], generating instability during cutting and impairing the surface integrity of microcomponent. Wu et al. [21] and Biermann et al. [22] reported that radius of the cutting edge increased with tool wear during micromilling, which, in turn, increased the rake angle and intensified the plowing mechanism. As a consequence, burr formation increased. Weule, Huntrup, and Tritschler [23] assert that micromilling of materials with higher hardness, as is the case with quenched and tempered AISI D2 steel, results in increased burr height and that this fact is mainly associated to higher tool wear rates. Pratap et al. [24] concluded that the higher micromilling forces result mainly from cutting edge wear. In this case, the increase in machining force is due to the plowing mechanism, which occurs when the feed per tooth is smaller than the minimum cutting thickness and leads to an increase in the passive force as a consequence of the size effect [25, 26].

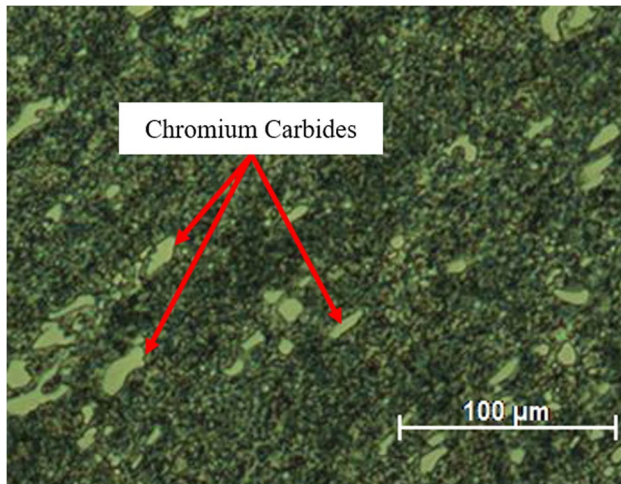
Gao et al. [27] analyzed the wear of a cutter using SEM, based on the change in tool diameter, while investigating micromilling of a single-crystal nickel-based superalloy DD98 using 600- μ m-diameter cemented carbide micromilling cutters. The tool was measured after the tests, and the influence of the cutting parameters was assessed. As the cutting speed, feed rate, and axial depth of cut increased, the wear mechanism and changes in the shape of the cutting tools became increasingly evident. Similar studies were conducted by Ziberov et al. [28] and Sorgato et al. [17], who used a similar method to measure wear in micromilling cutters during the machining of Ti-6Al-4V titanium alloy and Inconel 718 nickel alloy, respectively.

Gomes et al. [16] analyzed the wear of the 400- μ m carbide micro-endmill cutter during the micromilling of austenitic stainless steel AISI 316L using a support vector machine (SVM) model. The study presented a novel approach to monitor the cutter wear in micromilling operation by employing an artificial intelligence model to combine vibration and sound signals and learn a pattern for determining tool wear. The results showed that the SVM model was effective in determining the wear condition with an accuracy of up to 97.54%.

The novelty of this study lies in the investigation of the top burr height using the reduced peak height (Spk parameter) obtained from the Abbott-Firestone curve and its correlation with tool wear during micromilling of hardened AISI

Table 1 Chemical composition (wt.%) of AISI D2 steel [30]

Fe	C	Si	Cr	Mo	V
Balance	1.40–1.60	0.60 max	11.00–13.00	0.70–1.20	1.10 max

**Fig. 1** Microstructure of quenched and tempered AISI D2 steel

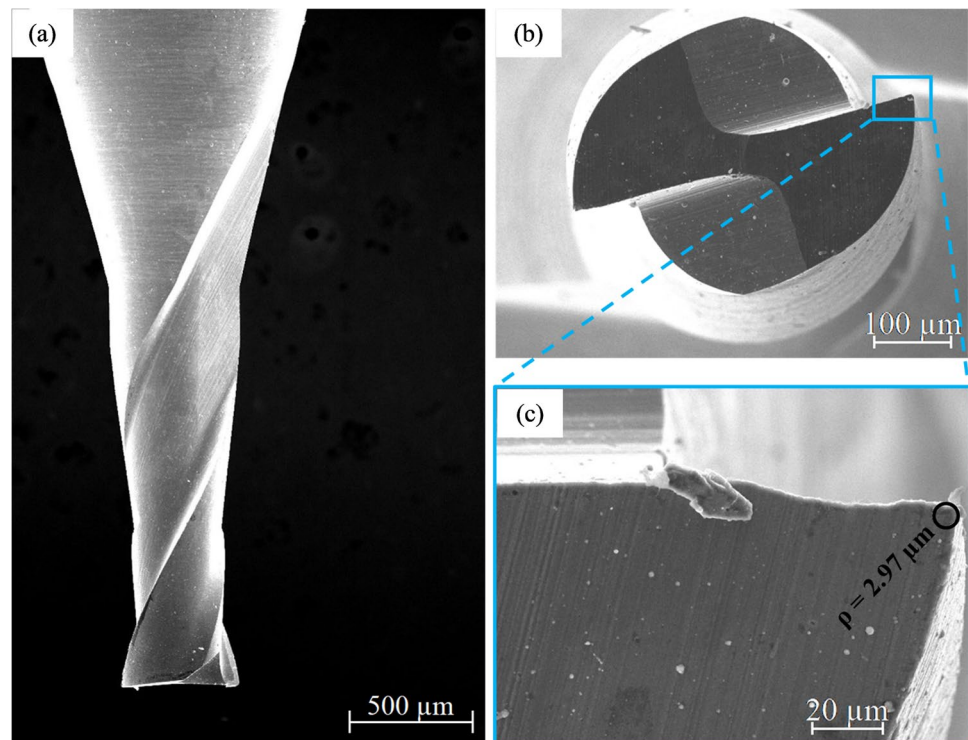
D2 steel. The tribological phenomena involved in micromilling can lead to the deterioration of the surface integrity of the produced microcomponents, as well as severe tool wear or premature tool failure, making the study of micromilling of AISI D2 steel particularly relevant. Therefore, the main

goal of this work is to investigate the effect of varying feed per tooth (3 and 6 μ m/tooth), axial depth of cut (20 and 40 μ m), and micromilling direction on burr formation when dry micromilling slots in quenched and tempered AISI D2 steel with an average hardness of 620 HV (57 ± 1 HRC). Furthermore, cutting tool wear and its influence on burr formation are investigated.

2 Materials and methods

Quenched and tempered AISI D2 steel with hardness of 620 ± 6 HV and dimensions $38 \times 38 \times 12$ mm is the work material used in the micromilling tests. The chemical composition is presented in Table 1, and Fig. 1 shows the microstructure of the work material, composed of chromium carbides distributed in a martensitic matrix. The tempering process in AISI D2 induces the precipitation of carbides (mainly M_7C_3) due to the high carbon content and content of alloying elements and since chromium content is high [29].

Micromilling tests were performed using TiAlN-coated carbide flat micro-endmills with two flutes, diameter of 500 μ m, and helix angle of 30° (Fig. 2a). The bottom view of the micro-endmill is shown in Fig. 2b and a detail of the secondary cutting edge highlighting the edge radius (ρ), with a value of approximately 2.97 μ m, is shown in Fig. 2c. Tool images were obtained with a Jeol JSM-IT300 SEM, and an

Fig. 2 Tool used in micromilling tests: **a** micro-endmill with a diameter of 500 μ m, **b** bottom view, and **c** detail of the cutting edge radius

Oxford Instruments X-MaxN EDS was used to perform EDS analyses on the clearance and rake faces of fresh and worn micro-endmills.

Micromilling tests were performed on a three-axis machining center, and the rotational movement of the micro-endmill was produced by a 650BT40 pneumatic turbine with power of 0.66 kW, maximum speed of 40,000 rpm, and working pressure of 6.2 bar. The micromilling force components were measured with a Kistler 9972 piezoelectric dynamometer connected to a Kistler 5073 signal amplifier and National Instruments 6366 data acquisition board (acquisition rate 25 kHz). F_x represents the micromilling force component perpendicular to the feed direction, F_y is the force component in the feed direction, and F_z is the axial (passive) force component. The experimental setup is shown in Fig. 3.

The selection of the machining parameters for the micromilling tests was based on the model proposed by Son et al. [31], which defines a minimum cutting thickness (t_m), thus allowing to minimize the size effect and reduce the action of the plowing mechanism. Such a model considers the minimum cutting thickness (t_m) as a function of the cutting tool edge radius (ρ) and the friction angle (β), as presented in Eq. 1.

$$t_m = \rho \left[1 - \left(\cos \frac{\pi}{4} - \frac{\beta}{2} \right) \right] \quad (1)$$

where β is friction angle between chip and tool rake face or the friction angle between workpiece material and tool clearance face, and therefore, is calculated as a function of the coefficient of friction (μ), according to Eq. 2.

$$\beta = \arctan \mu \quad (2)$$

The coefficient of friction was obtained through pin-on-disk tests performed on a Micro Photonics MT 60 tribometer, following ASTM G99-05 standard [32]. The coefficient of friction in machining is difficult to characterize due to the regions of adhesion and sliding in the chip-tool interface, which are affected by various factors such as material properties, machining conditions, tool geometry, and temperature [33]. Although the friction coefficient values obtained through this method may not be entirely representative of the machining conditions, it is commonly used to determine the critical cutting thickness through Eq. 2 [34].

The pin-on-disk tests were performed with TiNAl-coated carbide pins sliding against tempered and quenched AISI D2 steel disks with a normal load of 4 N. The test parameters employed were wear track diameter of 48 mm, sliding distance of 1000 m, test duration time of 180 min, and sliding speed equivalent to the cutting speed used in the micromilling tests (62.83 m/min). The results of the coefficient of friction versus sliding distance are shown in Fig. 4. The friction coefficients obtained under steady conditions (after 1000 m sliding distance) present an average value of 0.74 ± 0.05 . Blau [35] reports that the friction behavior curve is divided between running-in and the stationary regime (stable phase). Two bodies in contact under load and relative motion between them can induce changes on the surfaces that are detectable by the change in friction. In the initial phase of friction (running-in), contact occurs between the pin and the roughness peaks of the disk, which will undergo accelerated wear (emphasizing that the disk is designed so

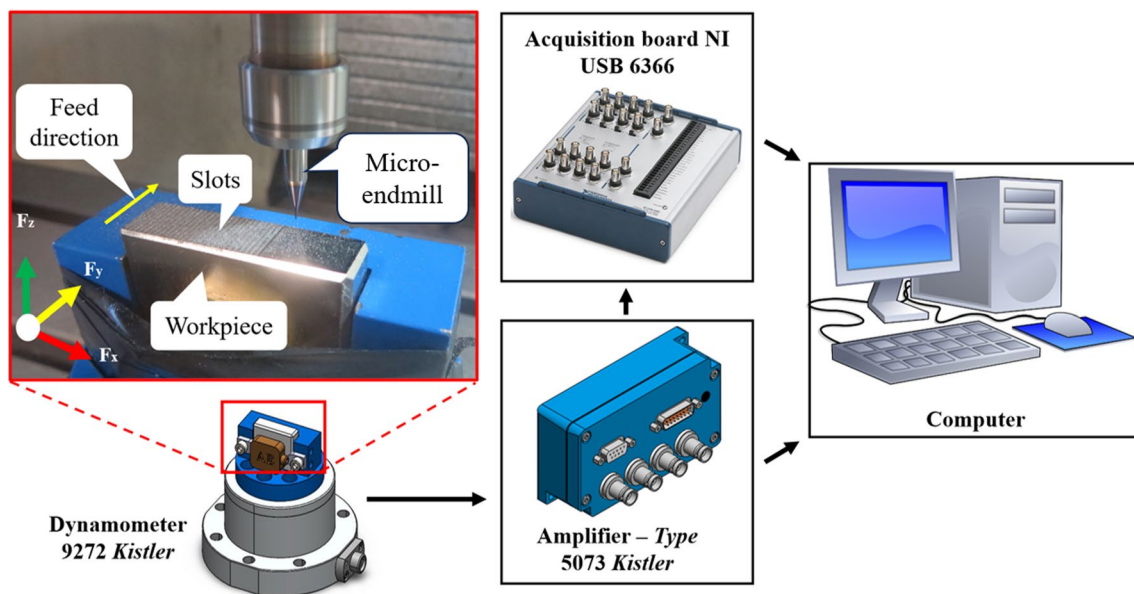


Fig. 3 Experimental configuration of micromilling tests

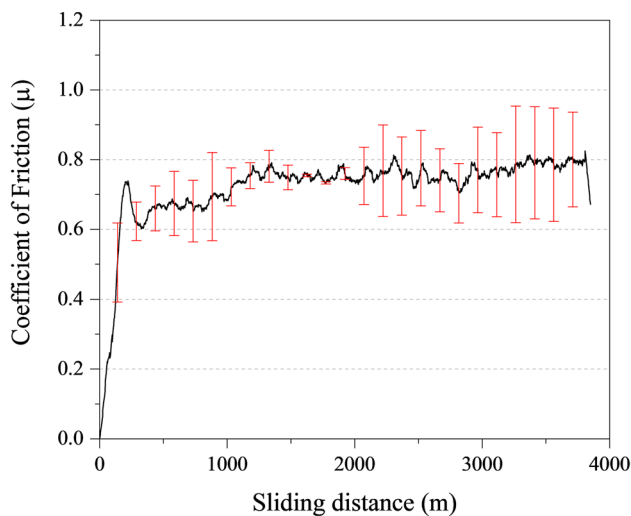


Fig. 4 Coefficient of friction versus sliding distance

that wear is concentrated on it), generating a progressive increase in the coefficient of friction. After the running-in period, there is a geometric accommodation of the pin-disk pair in which the average friction coefficient tends to remain relatively constant (steady state). From the values of the average coefficient of friction obtained empirically and considering a cutting edge with an average radius of $\rho = 2.97\mu\text{m}$, the minimum thickness of the material cut, calculated by Eq. 1, was approximately $1.72\mu\text{m}$. The feed per tooth must be higher than the minimum cutting thickness, because, as previously mentioned, it reduces the size effect and the plowing mechanism.

Based on the model proposed by Son et al. [31], see Eq. (1), it was possible to determine the minimum cutting thickness (t_m), used as a reference for the determination of the feed per tooth (f_z) employed in the micromilling tests. It is noteworthy that a feed per tooth lower than the minimum cutting thickness (t_m) induces the size effect and intensifies the plowing mechanism, leading to intense burr formation. Table 2 presents the parameters used in the micromilling tests.

Tool wear tests were performed with the parameters shown in Table 3 and using catastrophic failure as tool life criterion. The cutting parameters used in the wear tests were based on the machining conditions recommended by the cutting tool manufacturer.

The height and volume of top burrs were assessed using a Hommelwerk T8000 contact profilometer (Fig. 5a). For the top burr height measurements, five planes perpendicular to the tool feed direction were obtained (Fig. 5b), thus enabling the extraction of five profiles of the micromilled slots, as illustrated in Fig. 5c. The Abbott-Firestone curve was used to measure burr volume (Fig. 5d). The reduced peak height (Spk) parameter was used, which refers to the height of the

Table 2 Micromilling parameters

Parameter	Values
Feed per tooth, f_z ($\mu\text{m}/\text{tooth}$)	3 and 6
Axial depth of cut, a_p (μm)	20 and 40
Micromilling direction	Up and down
Cutting speed, v_c (m/min)	62.83
Micromilling length (mm)	387
Length per slot (mm)	9

peaks above the surface, from which the volume of the top burrs was obtained. The height of the top burrs was considered to be the distance from the surface of the sample to the highest peak present along the extracted plane (Fig. 5e). The method used to evaluate the height and volume of the top burr was based on the works of Malayath et al. [36] and Medeossi et al. [37]. The top burrs were evaluated on the left and right edges of the micromilled slots. Since micromilling of slots shows evidence that the burrs on each edge have different dimensions [38, 39], the parameters which characterize the burrs were evaluated in terms of the up and down micromilling cutting directions.

SEM analyses were also employed to evaluate micromilling tool wear mechanisms and to perform the characterization of the top burr width. Ultrasonic cleaning was necessary to obtain a better visualization of the tool wear region due to the presence of contaminants on the micromill surface. Acetone was used for ultrasonic cleaning of the tool in a Branson 1800 equipment. The measurement of the width of the top burrs formed by up and down micromilling cutting directions was performed in the SEM. For this purpose, 10 measurements were performed and the average value and standard deviation were calculated for each micromilling condition. Figure 6 represents the method used for measuring the burr width (W).

3 Results and discussion

3.1 Micromilling force components

The micromilling force components F_x , F_y , and F_z obtained for 387 mm micromilling length are shown in Fig. 7. Considering

Table 3 Micromilling parameters used in the tool life tests

Parameter	Values
Feed per tooth, f_z ($\mu\text{m}/\text{tooth}$)	13.2
Axial depth of cut, a_p (μm)	17
Cutting speed, v_c (m/min)	62.83
Length per slot (mm)	9

Fig. 5 Profilometry of the samples: **a** scanning of the micro-machined sample; **b** planes perpendicular to the feed direction to extract the slots profiles; **c** measurement of the top burr height; **d** Abbott-Firestone curve; **e** top burrs obtained for the calculation of the top burr volume

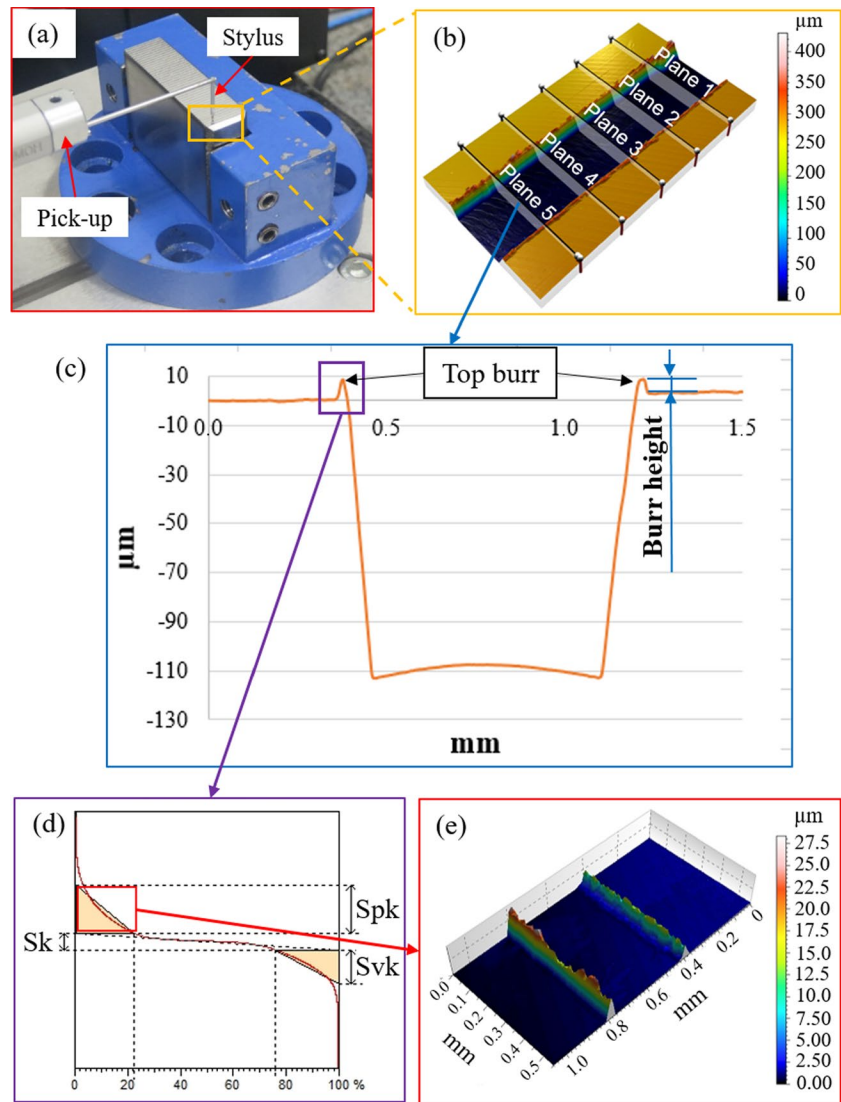
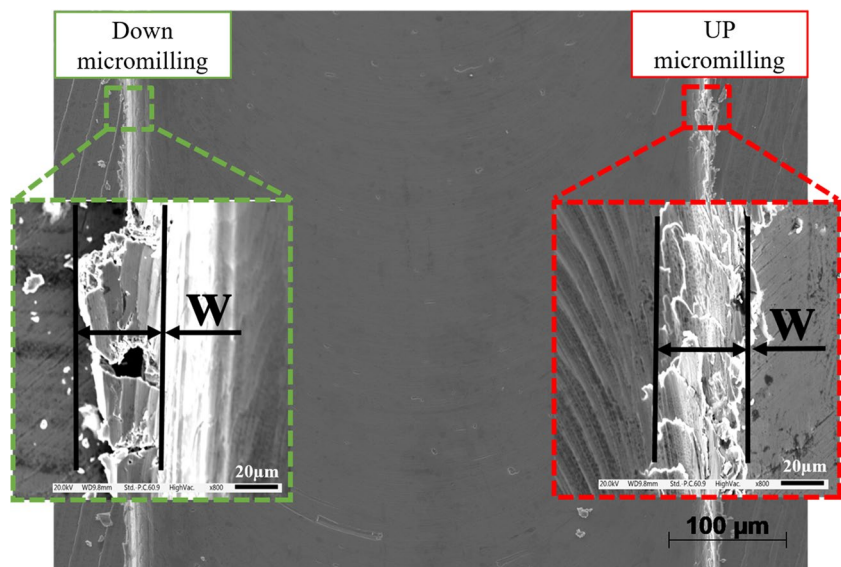


Fig. 6 Measurement of the width of the top burrs for the up and down micromilling cutting direction



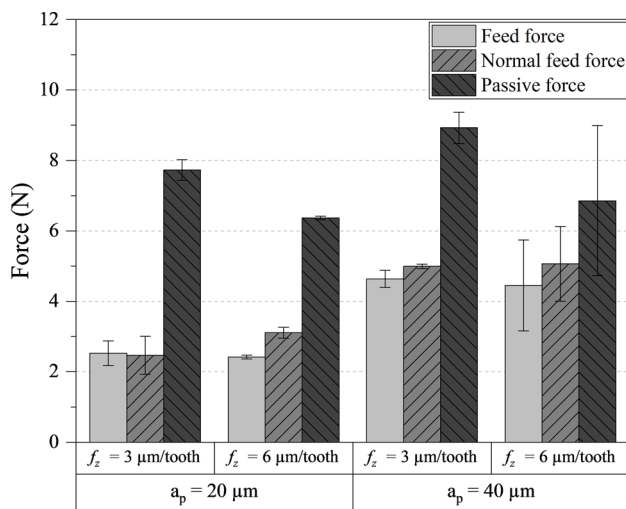


Fig. 7 Radial (F_x), feed (F_y), and passive (F_z) components of the micromilling force

the influence of feed per tooth (f_z) and axial depth of cut (a_p) on the F_x component, it can be noticed that increasing feed per tooth from 3 to 6 $\mu\text{m/tooth}$ does not cause a significant difference when the axial depth of cut is kept constant. The F_x component only increased when a_p increased from 20 to 40 μm for the same f_z . This behavior can be explained by the increase in the volume of material removed with the increase in the axial depth of cut. Similar results were reported by Uzun et al. [40]. The machining component F_y showed similar behavior to that found in F_x , i.e., only axial depth of cut presented a significant effect on the force intensity. For all machining conditions tested, the micromilling component F_z achieved the highest values compared with the F_x and F_y components, corresponding to a force increase of approximately 31% and 32%, respectively. This fact is related to the wear of the cutting edge of the tool during micromilling of the slots. Rounding the cutting edge changes the f_z/ρ ratio (ratio of the feed per tooth to the edge radius) and the chip thickness, which explains the increase of F_z , since the rounding of the cutting edge will produce chips with thinner thicknesses (size effect) and intensification of the plowing mechanism. This generates a higher resistance to tool movement, thus increasing the passive cutting force. Similar behavior was observed by Gao et al. [41], who reported that increased tool wear altered the tool rake angle, tending to make it negative and which significantly affected the F_z component of the micromilling force.

3.2 Influence of micromilling parameters on the formation of top burrs

Figure 8 shows the top burrs formed in the up and down cutting directions and Table 4 presents the results of analysis of

variance (ANOVA) for top burr height considering micromilling direction, f_z and a_p at a confidence level of 95%. It can be seen that a_p , $f_z * a_p$ interaction, f_z and micromilling direction (Md), in this order, significantly affected the top burr height. The R^2 value obtained in this study indicates that approximately 93% of the top burr height can be explained by the statistical model adopted.

The most relevant factor to the increase in burr height is axial depth of cut (a_p). By doubling a_p , burr height increased approximately 400%. This fact is related to the higher volume of material removed, which requires higher micromilling forces to remove the chip by shear, leading to wear of the cutting edge and resulting in a more negative rake angle. As a consequence, plowing becomes more intense, possibly resulting in incomplete chip flow and, therefore, higher amounts of burrs. These findings agree with those reported by [42]. Feed per tooth also contributes to a change in burr height. By doubling f_z , the burr height is reduced by approximately 26%. Increasing f_z positively affects burr formation, as its increase minimizes the deleterious effect of the material plowing. Down micromilling promoted a top burr height approximately 23% higher in relation to up cutting direction, corroborating Aramcharoen and Mativenga [43]. The elevation of top burr height observed when down cutting may be related to the larger volume of plastically deformed material generated ahead of the cutting edge, when displaced to the edge of the slot, breaks through fracture in the upper part of the slot, keeping a portion of material attached to the workpiece [44]. Figure 9 shows the behavior of the top burr height with micromilling length and variations on the parameters f_z and a_p .

From Fig. 9a to d, it can be observed that down micromilling generally showed the highest burr height compared to up micromilling. There is also a transition in the behavior of the burr height for the down and up micromilling cutting directions starting from a machining length of 200 mm, suggesting that the wear of the micro-endmill may have influenced the higher burr height values. However, this behavior was not observed in Fig. 9d, where down micromilling showed a tendency of increasing burr heights while for up micromilling it remained constant. This result suggests that due to the oscillatory behavior of the burr height, it was not possible to observe any difference in height after a machining length of 387 mm. A similar behavior was observed in Fig. 9a, where the burr height increased and decreased as a function of the machining length. Thus, it is suggested that for a longer machining length, it would be possible to observe a difference in burr height for the up micromilling (Fig. 9d). A similar behavior was observed by [45].

The top burr height distributions (burr height/ mm^2) are presented in histograms obtained by means of the contact profilometer (Fig. 10). Peak count distribution histograms indicate the number of burrs (areas corresponding to top

Fig. 8 Top burrs for up and down cutting directions with distinct f_z and a_p values

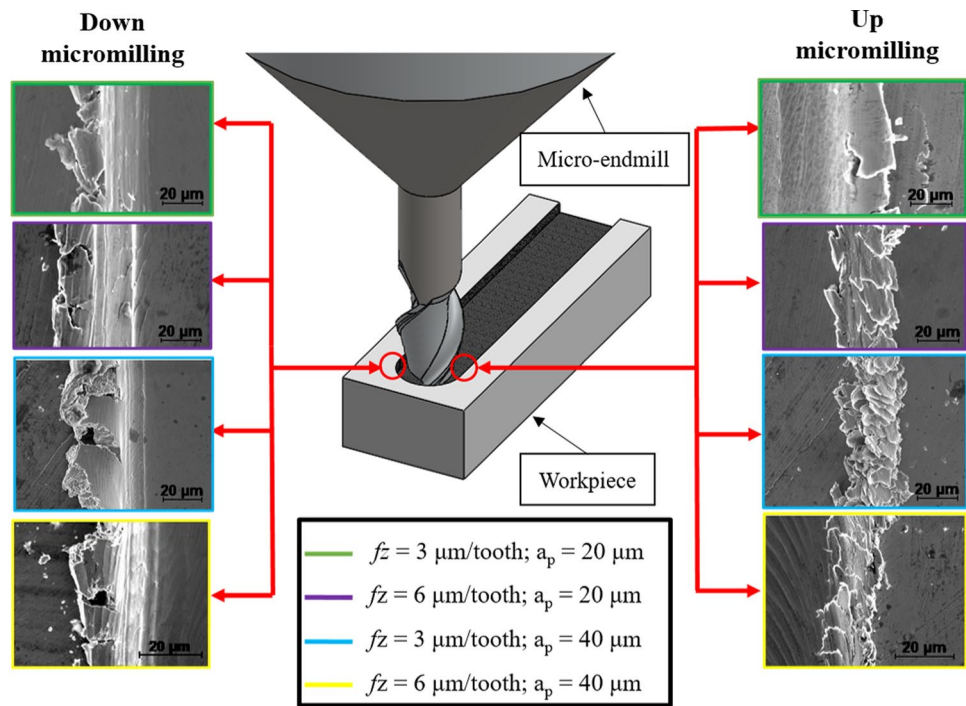


Table 4 Analysis of variance (ANOVA) for top burr height

Source	DF	Seq SS	Contribution	Adj SS	Adj MS	P-value
Model	7	96,095	93.04%	96,094.8	13,727.8	0.000
Linear	3	89,978	87.11%	89,978.2	29,992.7	0.000
a_p (μm)	1	81,225	78.64%	81,225.2	81,225.2	0.000
f_z ($\mu\text{m}/\text{tooth}$)	1	5038	4.88%	5037.8	5037.8	0.000
Md	1	3715	3.60%	3715.3	3715.3	0.000
2-way interactions	3	6115	5.92%	6115.3	2038.4	0.000
$f_z * a_p$	1	5455	5.28%	5454.6	5454.6	0.000
$a_p * \text{Md}$	1	660	0.64%	660.2	660.2	0.096
$f_z * \text{Md}$	1	1	0.00%	0.6	0.6	0.959
3-way interactions	1	1	0.00%	1.3	1.3	0.941
$f_z * a_p * \text{Md}$	1	1	0.00%	1.3	1.3	0.941
Error	32	7193	6.96%	7192.9	224.8	
Total	39	103,288	100.00%			
Model summary						
S	R^2	R^2 (adj.)	R^2 (pred)			
14.9926	93.04%	91.51%	89.12%			

burrs) that are situated above the machining plane, i.e., the number of top burrs per unit area.

For micromilling performed with $f_z = 3 \mu\text{m}/\text{tooth}$ and $a_p = 20 \mu\text{m}$ (Fig. 10a), a burr height ranging between 10 and 60 μm was observed, with a burr distribution of 2.50 burrs/ mm^2 for a height of 42 μm . In contrast, $f_z = 6 \mu\text{m}/\text{tooth}$ and $a_p = 20 \mu\text{m}$ (Fig. 10b) exhibited a burr height between 30 and 100 μm , together with a distribution of 4.46 burrs/ mm^2 for a height of 36.86 μm . Comparing Fig. 10a and b, the burr heights remained similar. However, with increased feed per

tooth, a larger quantity of burrs/ mm^2 was formed, indicating a higher volume of chips generated during micromilling. This phenomenon is a direct result of the higher feed per tooth, leading to a higher material removal rate and subsequently larger volumes of burrs. Figure 10c shows that a burr height ranging between 70 and 180 μm was observed, with a burr distribution of 2.30 burrs/ mm^2 for a height of 130 μm . In Fig. 10d, the burr height ranged from 50 to 160 μm , with a burr distribution of 4.30 burrs/ mm^2 for a height of 88 μm . The machining condition with $f_z = 3 \mu\text{m}/\text{tooth}$ and $a_p = 40$

Fig. 9 Top burr height in up and down direction for **a** $f_z = 3 \mu\text{m}/\text{tooth}$ and $a_p = 20 \mu\text{m}$, **b** $f_z = 6 \mu\text{m}/\text{tooth}$ and $a_p = 20 \mu\text{m}$, **c** $f_z = 3 \mu\text{m}/\text{tooth}$ and $a_p = 40 \mu\text{m}$, and **d** $f_z = 6 \mu\text{m}/\text{tooth}$ and $a_p = 40 \mu\text{m}$

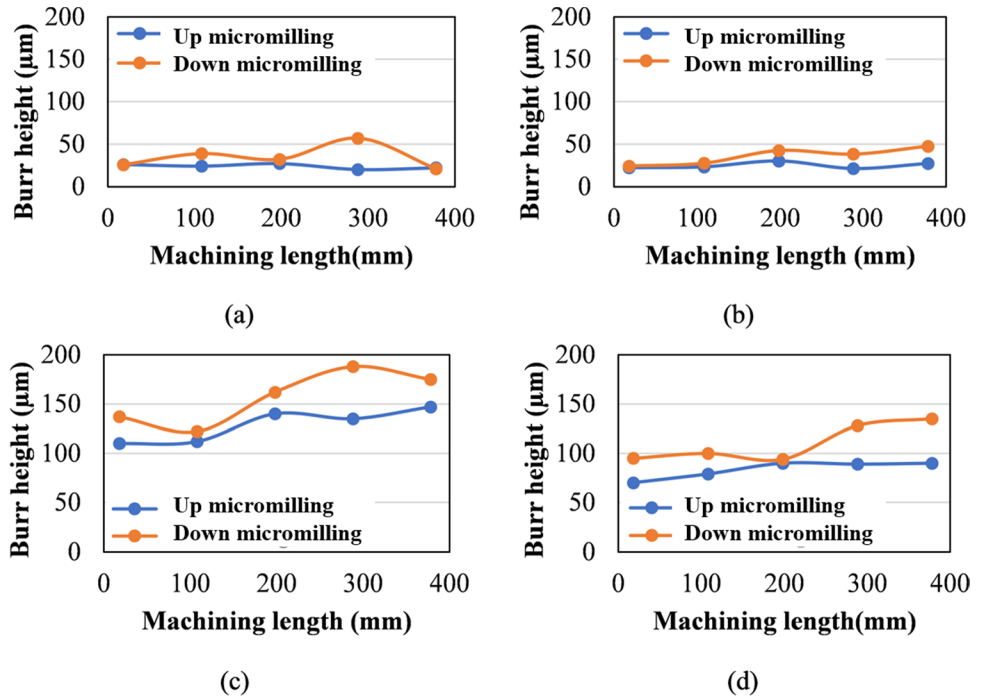
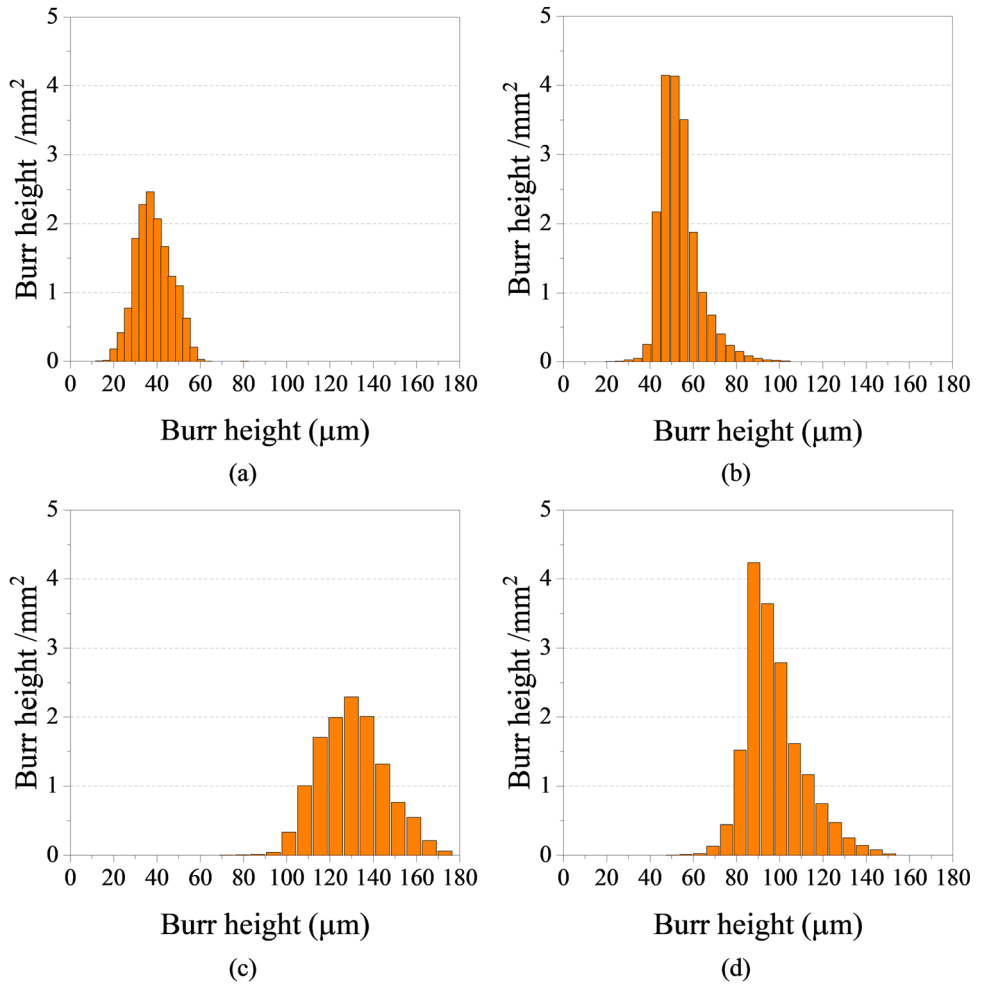


Fig. 10 Top burr height histogram for **a** $f_z = 3 \mu\text{m}/\text{tooth}$ and $a_p = 20 \mu\text{m}$, **b** $f_z = 6 \mu\text{m}/\text{tooth}$ and $a_p = 20 \mu\text{m}$, **c** $f_z = 3 \mu\text{m}/\text{tooth}$ and $a_p = 40 \mu\text{m}$, and **d** $f_z = 6 \mu\text{m}/\text{tooth}$ and $a_p = 40 \mu\text{m}$



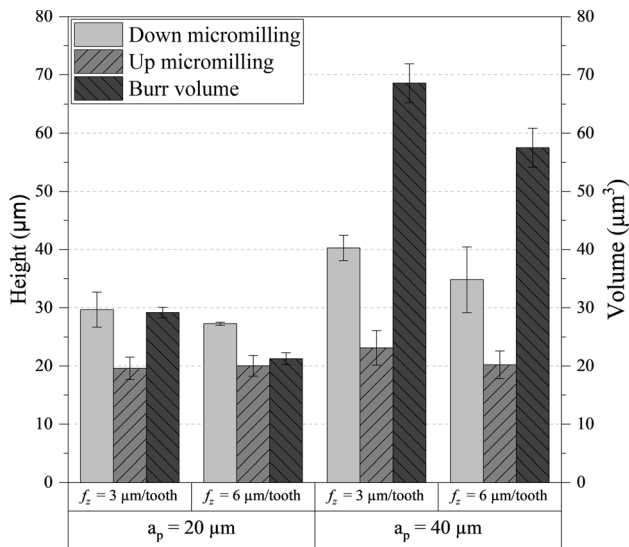
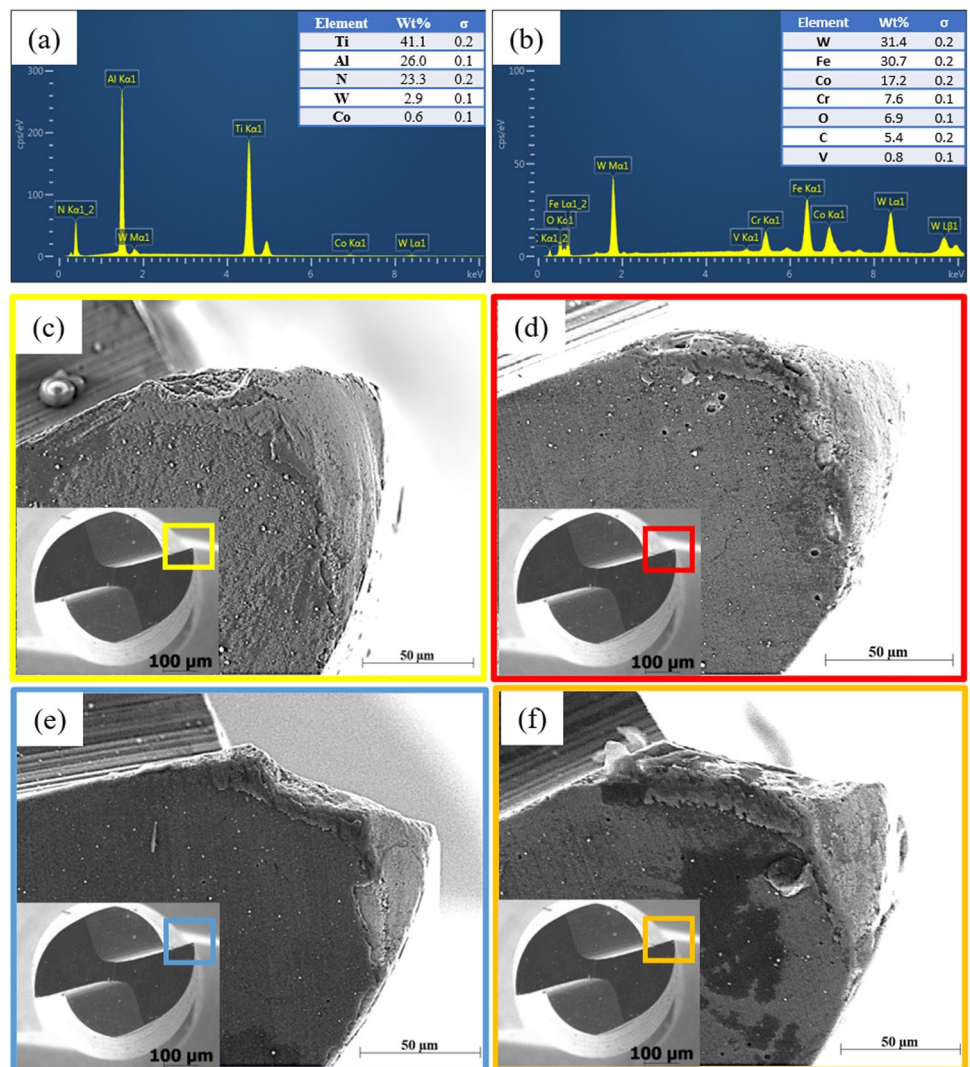


Fig. 11 Height and volume of the top burr

μm resulted in increased burr height compared to $f_z = 6 \mu\text{m/tooth}$ and $a_p = 40 \mu\text{m}$. However, the $f_z = 3 \mu\text{m/tooth}$ and $a_p = 40 \mu\text{m}$ condition presented lower burrs/mm² compared to $f_z = 6 \mu\text{m/tooth}$ and $a_p = 40 \mu\text{m}$. In other words, the $f_z = 3 \mu\text{m/tooth}$ and $a_p = 40 \mu\text{m}$ condition produced increased burr height but in a reduced quantity burrs/mm² compared to the $f_z = 6 \mu\text{m/tooth}$ and $a_p = 40 \mu\text{m}$ condition.

When comparing Fig. 10a and c, it was observed that keeping the f_z constant and increasing the a_p from 20 to 40 μm lead to an increase in the burr height, while the difference in distribution of burrs/mm² remains negligible. Figure 10c and d present a similar behavior. In micromilling, a lower f_z generally results in an increased burr height due to prolonged tool-work material contact, increased friction, and cutting edge wear. Conversely, a higher f_z tends to reduce burr height and increase the amount of burrs/mm². With the increase in a_p from 20 to 40 μm, an increase in burr height was observed due to the larger volume of material removed from the workpiece.

Fig. 12 Micro-endmill analysis: EDS of the tool a before and b after micromilling, and tool wear analysis after micromilling 387 mm at c $f_z = 3 \mu\text{m/tooth}$ and $a_p = 20 \mu\text{m}$, d $f_z = 6 \mu\text{m/tooth}$ and $a_p = 20 \mu\text{m}$, e $f_z = 3 \mu\text{m/tooth}$ and $a_p = 40 \mu\text{m}$, and f $f_z = 6 \mu\text{m/tooth}$ and $a_p = 40 \mu\text{m}$



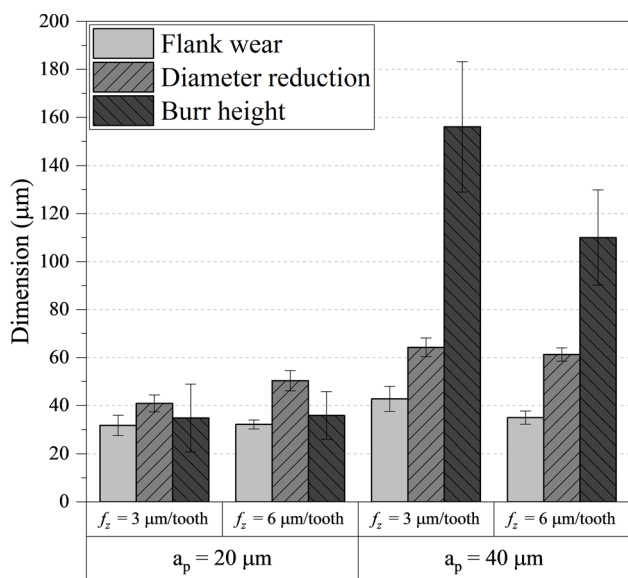


Fig. 13 Relationship between tool wear (flank wear and tool diameter reduction) and top burr height after micromilling for 387 mm under distinct feeds per tooth (f_z) and axial depths of cut (a_p)

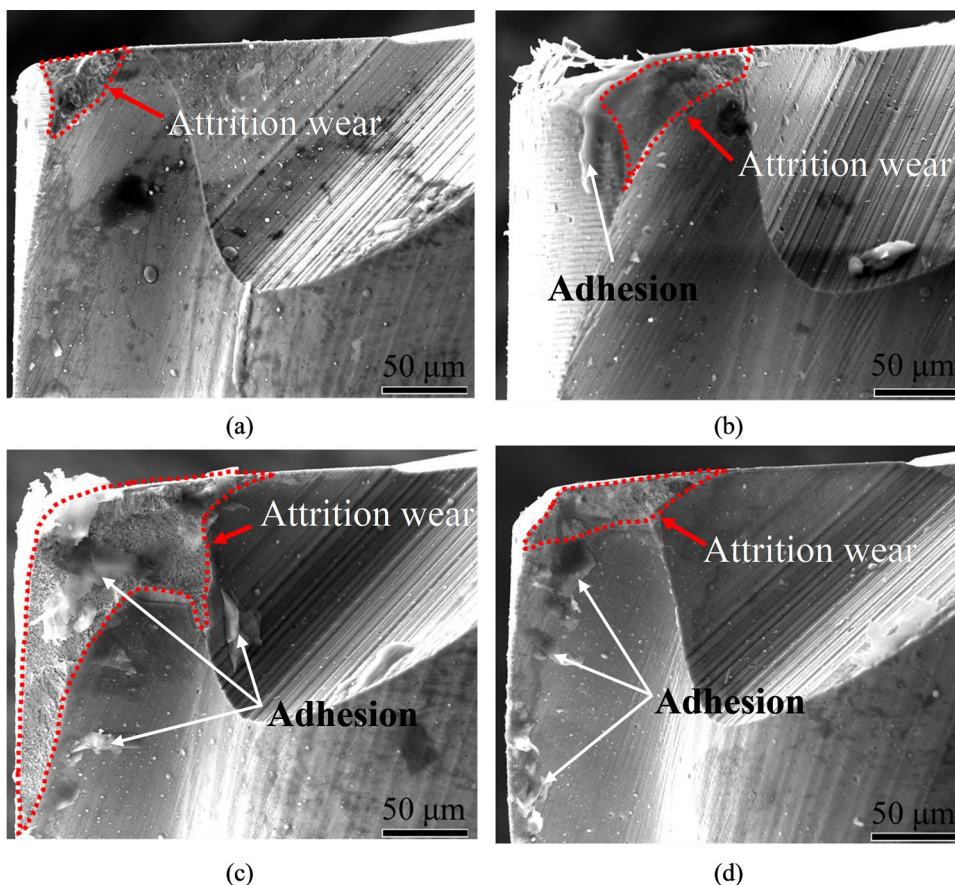
The average values of the top burr width, obtained by means of SEM and statistically treated by the paired t -test, are presented in Fig. 11. The statistical analysis indicated that

the difference is statistically significant (p -value = 0.006). When down cutting, the width of the top burrs is higher than in the up cutting direction. The highest burr width is generated when micromilling is performed with $f_z = 3 \mu\text{m}/\text{tooth}$ and $a_p = 40 \mu\text{m}$. This can be explained by the larger volume of material removed and the higher tool wear for this condition. Regarding tool wear, which will be detailed in the next section, the highest flank wear was higher which was recorded for this condition. Therefore, flank wear may have contributed to increase the radius of the cutting edge, which in turn induced the plowing mechanism, which implies in higher plastic deformation, thus resulting in higher burrs.

3.3 Effect of micromilling tool wear on the formation of top burrs

Chemical analyses of the surface of the micro-endmill, before and after micromilling (performed with $f_z = 3 \mu\text{m}/\text{tooth}$ and $a_p = 20 \mu\text{m}$ in a machining length of 387 mm), are shown in Fig. 12a and b, respectively. The EDS analysis of the tool before micromilling identified only the presence of tungsten, titanium, nitrogen, aluminum, and cobalt, elements that make up the micromilling cutter substrate and TiAlN coating. The EDS of the micro-endmill

Fig. 14 Attrition wear analysis of the tool after micromilling at **a** $f_z = 3 \mu\text{m}/\text{tooth}$ and $a_p = 20 \mu\text{m}$, **b** $f_z = 6 \mu\text{m}/\text{tooth}$ and $a_p = 20 \mu\text{m}$, **c** $f_z = 3 \mu\text{m}/\text{tooth}$ and $a_p = 40 \mu\text{m}$, and **d** $f_z = 6 \mu\text{m}/\text{tooth}$ and $a_p = 40 \mu\text{m}$



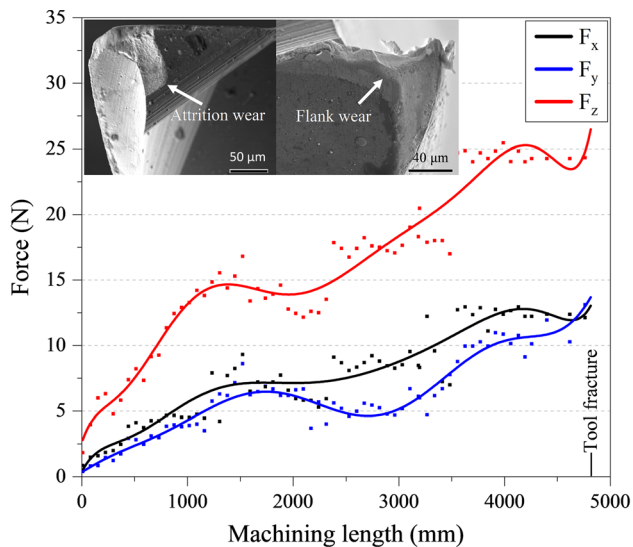


Fig. 15 Micromilling force components evolution with machining length (tool wear)

after micromilling also indicates the presence of chromium and vanadium from the workpiece material that remained adhered to the cutting edge, suggesting the occurrence of adhesive wear. In Fig. 12c, $f_z = 3 \mu\text{m/tooth}$ and $a_p = 20 \mu\text{m}$ were used, while in Fig. 12d, the values were $f_z = 6 \mu\text{m/tooth}$ and $a_p = 20 \mu\text{m}$. Both figures exhibit signs of wear on the cutting edge of the micro-endmill. In Fig. 12e and f, the machining conditions were $f_z = 3 \mu\text{m/tooth}$ and $a_p = 40 \mu\text{m}$, and $f_z = 6 \mu\text{m/tooth}$ and $a_p = 40 \mu\text{m}$, respectively. In these cases, there is noticeable more pronounced wear on the cutting edge compared to Fig. 12c and d. Figure 12c to f present the images obtained by means of SEM of the micro-endmills after machining. Work material adhered to the tool clearance surface can be observed and similar results were

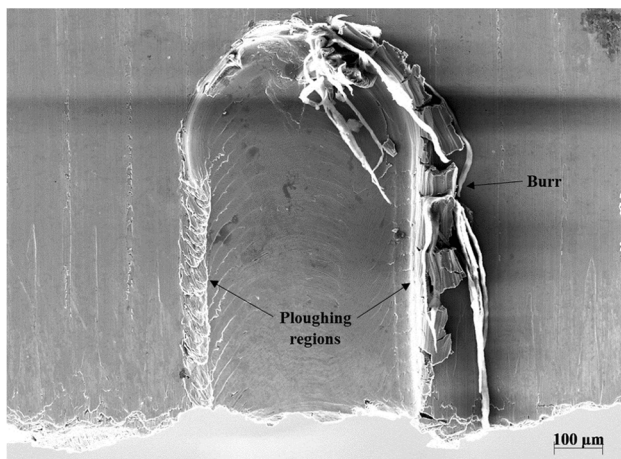


Fig. 16 SEM images of the region where the tool fractured

found by Silva and Silva [19]. These results suggest that adhesion is the mechanism responsible for tool wear. This was caused by the thermal softening and viscoplastic flow of AISI D2 as a result of the increased cutting temperature due to friction and plastic deformation involved in machining. The high hardness of the material requires higher forces to promote plastic deformation, leading to an increase in local temperature. As the temperature rises during micromilling, AISI D2 steel exhibits a viscoplastic behavior, and adheres to the tool surface under intense pressure [46].

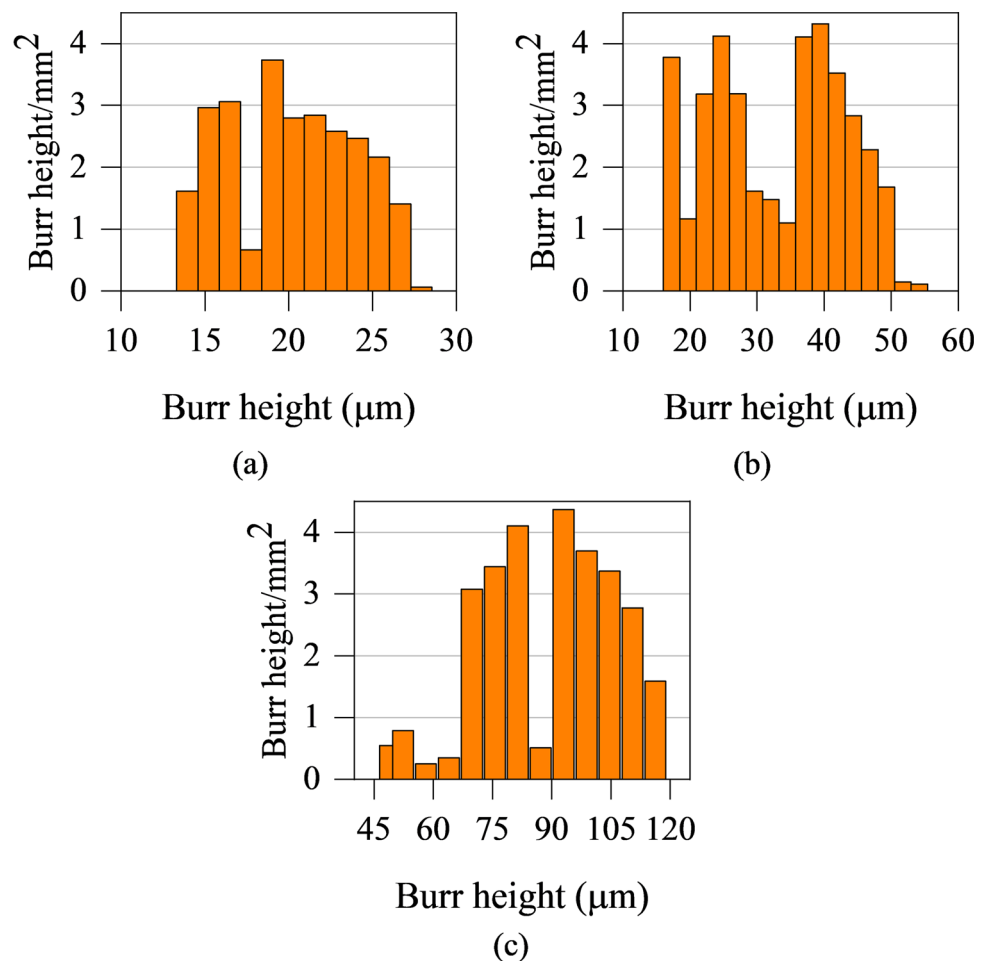
Adhesive wear can be described by a periodic cycle. After the cutting edges of the tool performed their first machining path, a portion of material adhered to the surface of the micro-endmills was observed. During the cut, this material adhered to the tool comes into contact with the work material, being compressed and, consequently. Subsequently, the adhered and work hardened material is detached from the tool surface, tearing the material of the cutting edge, and, consequently, changing the geometry of the cutting tool. The peeling of the adhesive materials caused the tool material in direct contact to be torn, further weakening the cutting edge and leading to catastrophic broken. This phenomenon can elevate temperature and the components of the micromilling force, leading to the increase of the passive force component. Additionally, tool wear contributes to the formation burrs.

Figure 13 presents the relationship between tool wear (flank wear and diameter reduction) and burr height after micromilling 387 mm using distinct feeds per tooth and axial depths of cut. Burr formation is more pronounced for $f_z = 3 \mu\text{m/tooth}$ and $a_p = 20 \mu\text{m}$. The results suggest that the increase in flank wear and the reduction in the diameter of the micro-endmill promote a change in the chip-tool interface that affects chip formation, hindering shearing, and inducing plowing. As a consequence, a portion of the material that is not removed in the form of a chip remains as a burr on the slot edge.

Figure 14 shows the rake face of the micro-endmill. Upon analyzing Fig. 14a through d, wear on the rake face was observed. For all the tested conditions, the occurrence of the attrition mechanism is suggested, which is the result of contact between the cutting tool and the machined material. This is due to friction and abrasion between the cutting edge of the end mill and the material, resulting in gradual wear on the rake face surface.

Comparing Fig. 14a and b, it is possible to observe that both exhibit similar wear patterns. On the other hand, when comparing Fig. 14c and d, with $f_z = 3 \mu\text{m/tooth}$ and $a_p = 40 \mu\text{m}$, and $f_z = 6 \mu\text{m/tooth}$ and $a_p = 40 \mu\text{m}$, respectively, it is evident that the former exhibited larger wear. This behavior reflected in the burr height (Fig. 13), where the machining conditions $f_z = 3 \mu\text{m/tooth}$ and $a_p = 20 \mu\text{m}$, and $f_z = 6 \mu\text{m/tooth}$ and $a_p = 20 \mu\text{m}$, resulted in similar burr heights. Conversely, the machining conditions f_z

Fig. 17 Burr height distribution histogram for $f_z = 3 \mu\text{m}/\text{tooth}$ and $a_p = 20 \mu\text{m}$ for machining lengths of **a** 1600 mm, **b** 4000 mm, and **c** 4875 mm



$= 3 \mu\text{m}/\text{tooth}$ and $a_p = 40 \mu\text{m}$, and $f_z = 3 \mu\text{m}/\text{tooth}$ and $a_p = 40 \mu\text{m}$, led to different burr heights, with the highest burr height and largest wear observed for $f_z = 3 \mu\text{m}/\text{tooth}$ and $a_p = 40 \mu\text{m}$.

Tool wear evolution was monitored during micromilling at $f_z = 13.20 \mu\text{m}/\text{tooth}$ and $a_p = 17 \mu\text{m}$ by means of the force signals. Tool fracture was adopted as the end-of-life criterion. Figure 15 details the gradual increase in the radial, feed, and passive forces as a function of the machined length.

A gradual increase in the micromilling force components can be seen as the machining length increases. This occurs due to the increased contact at the tool-workpiece interface that generates higher friction and, consequently, increased wear. The tool fractured after a machining length of approximately 4815 mm, reaching the maximum radial force of 12 N, feed force of 12 N, and passive force of 23 N. The fact that the F_z component shows a higher value when compared with the F_y and F_x components can be attributed to the plowing mechanism of the material. Figure 16 shows a SEM image of the region where the tool fractured. It is possible to note the presence of burr and plowing regions.

Finally, the relationship between top burr height distributions (burr height/mm²) and burr height was evaluated for machining lengths of 1600, 4000, and 4815 mm (Fig. 17). It is observed that, for the machining lengths of 1600, 4000, and 4815 mm, the heights of the top burrs presented values in the intervals of 14 to 28 μm (Fig. 17a), 17 to 55 μm (Fig. 17b), and 49 to 119 μm (Fig. 17c), respectively. This result suggests that as the machining length increases, chip formation by shearing is no longer predominant, as the minimum thickness to form the chip decreases due to changes in tool cutting edge geometry, leading to an increasing radius of the cutting tool edge, with a consequent increase in burr formation. Thus, the material that was not removed by shearing turned into burr being pushed by the cutting edge of the tool to the sides of the slot.

4 Conclusion

After subjecting hardened AISI D2 steel to micromilling under various conditions, the conclusions below can be drawn.

Regarding the micromilling force, the radial and feed components of the micromilling force were lower than the passive force, which indicates plowing, resulting in the formation of top burrs. For all evaluated machining conditions, the micromilling component F_z reached the highest values compared to the F_x and F_y components, corresponding to an increase of approximately 31% and 32%, respectively. This fact is related to the wear of the cutting edge of the tool during micromilling of the slots.

Regarding the formation of top burrs, axial depth of cut was the parameter that most influenced the increase in burr formation. Increasing the axial depth of cut (a_p) from 20 to 40 μm resulted in an approximately 400% increase in burr height, due to the larger volume of material removed and the higher forces required.

Increasing the feed per tooth (f_z) contributed to a reduction of approximately 26% in burr height, minimizing the detrimental effect of material plowing.

Micromilling in the down micromilling direction resulted in a burr height approximately 23% higher compared to the up micromilling direction.

As far as tool wear is concerned, attrition was the predominant wear mechanisms. The increase in tool wear along the machined length promoted an increase in all the components of the micromilling force. It is also noteworthy that the passive force was higher than the radial and feed forces. These facts are attributed to the rounding and the increase in the radius of the cutting edge, which tends to produce a negative rake angle, inducing the size effect and intensifying plowing.

Acknowledgements The authors are grateful to the Graduate Program in Mechanical Engineering, Universidade Federal de Minas Gerais and the Brazilian research agencies CAPES, CNPq, and FAPEMIG for financial support.

Author contribution Anderson Júnior dos Santos performed the micromilling test, scanning electron microscopy, and profilometry tests and wrote the main text. Bárbara Cristina Mendanha Reis editing and proofreading the article, Natália Fernanda Santos Pereira contributed to the data analysis, Diogo Azevedo de Oliveira article review, Alexandre Mendes Abrão article review, Juan Carlos Campos Rubio article review, and Marcelo Araújo Câmara is the leader of the research team and contributed to the analysis of the results and review of the article.

Funding This study was partly financed in part by the Coordenao de Aperfeioamento de Pessoal de Nvel Superior — Brasil (CAPES) — Finance Code 001.

Data availability Not applicable.

Code availability Not applicable.

Declarations

Ethics approval Not applicable.

Consent to participate All the authors consent to participate in this research.

Consent for publication The authors give full consent to the publisher for the publication of this work.

Competing interests The authors declare no competing interests.

References

- Chen N, Li H, Wu J, Li Z, Li L, Liu G, He N (2021) Advances in micromilling: From tool fabrication to process outcomes. *Int J Mach Tools Manuf* 160. <https://doi.org/10.1016/j.ijmactools.2020.103670>. Publisher Copyright: © 2020 Elsevier Ltd
- Mamedov A (2021) Micro milling process modeling: a review. *Manufacturing Rev* 8:3. <https://doi.org/10.1051/mfreview/2021003>
- Aramcharoen A, Mativenga PT, Yang S, Cooke KE, Teer DG (2008) Evaluation and selection of hard coatings for micro milling of hardened tool steel. *Int J Mach Tools Manuf* 48(14):1578–1584. <https://doi.org/10.1016/j.ijmactools.2008.05.011>
- Beruides G, No FC, Quiza R, Haber RE (2016) Surface roughness modeling and optimization of tungstencopper alloys in micro-milling processes. *Measurement* 86:246–252. <https://doi.org/10.1016/j.measurement.2016.03.002>
- Saedon JB, Soo SL, Aspinwall DK, Barnacle A (2012) Micro-milling of hardened aisi d2 tool steel. *Adv Mater Res* 445:62–67. <https://doi.org/10.4028/www.scientific.net/amr.445.62>
- Bodziak S, de Souza AF, Rodrigues AR, Diniz AE, Coelho RT (2014) Surface integrity of moulds for microcomponents manufactured by micromilling and electro-discharge machining. *J Braz Soc Mech Sci Eng* 36:623–635
- Sredanovic B, Lakic GG, Kramar D, Kopac J (2016) Analysis of micro-milling of hardened tool steel in key engineering materials. *Key Eng Mater* 686:57–62. <https://doi.org/10.4028/www.scientific.net/kem.686.57>
- Câmara MA, Rubio JCC, Abrão AM, Davim JP (2012) State of the art on micromilling of materials, a review. *J Mater Sci Technol* 28(8):673–685. [https://doi.org/10.1016/S1005-0302\(12\)60115-7](https://doi.org/10.1016/S1005-0302(12)60115-7)
- Yuan Z, Fang B, Zhang Y, Wang F (2022) Effect of cutting parameters on chips and burrs formation with traditional micromilling and ultrasonic vibration assisted micromilling. *Int J Adv Manuf Technol* 119:1–14. <https://doi.org/10.1007/s00170-021-08468-3>
- Li P, Aristimuno P, Arrazola P, Hoogstrate AM, Oosterling JAJ, Langen HH, Schmidt RHM (2008) A study of factors affecting the performance of micro square endmills in milling of hardened tool steels. In: *Proc 4th Int Conf Multi-Material Micro Manuf* 2008:1–4
- Kang IS, Kim JS, Kim JH, Kang MC, Seo YW (2007) A mechanistic model of cutting force in the micro end milling process. *J Mater Process Technol* 187–188:250–255. <https://doi.org/10.1016/j.jmatprotec.2006.11.155>. (3rd International Conference on Advanced Forming and Die Manufacturing Technology)
- Sun H, Gao D, Zhao Z, Tang X (2017) An approach to in-process surface texture condition monitoring. *Robot Comput-Integr Manuf* 48:254–262. <https://doi.org/10.1016/j.rcim.2017.05.001>
- Bajpai V, Singh RK, Kushwaha AK (2013) Burr formation and surface quality in high speed micromilling of titanium alloy (Ti6Al4V). *Int Manuf Sci Eng Conf Am Soc Mech Eng* 2013:V002T03A017

14. Biermann D, Kahnis P (2010) Analysis and simulation of size effects in micromilling. *Prod Eng Res Devel* 4:25–34. <https://doi.org/10.1007/s11740-009-0201-1>
15. Chen MJ, Ni HB, Wang ZJ, Jiang Y (2012) Research on the modeling of burr formation process in micro-ball end milling operation on Ti-6Al-4V. *Int J Adv Manuf Technol* 62(9–12):901–912. <https://doi.org/10.1007/s00170-011-3865-6>
16. Gomes MC, Brito LC, da Silva MB, Viana Duarte MA (2021) Tool wear monitoring in micromilling using support vector machine with vibration and sound sensors. *Precis Eng* 67:137–151. <https://doi.org/10.1016/j.precisioneng.2020.09.025>
17. Sorgato M, Bertolini R, Bruschi S (2020) On the correlation between surface quality and tool wear in micromilling of pure copper. *J Manuf Process* 50:547–560. <https://doi.org/10.1016/j.jmapro.2020.01.015>
18. Bal'azs BZ, Geier N, Tak'acs M, Davim JP (2021) A review on micromilling: recent advances and future trends. *Int J Adv Manuf Technol* 112:655–684
19. Silva LC, da Silva MB (2019) Investigation of burr formation and tool wear in micromilling operation of duplex stainless steel. *Precis Eng* 60:178–188. <https://doi.org/10.1016/j.precisioneng.2019.08.006>
20. Kiswanto G, Zariatin D, Ko T (2015) The effect of spindle speed, feed-rate and machining time to the surface roughness and burr formation of aluminum alloy 1100 in micro-milling operation. *J Manuf Process* 16(4):435–450. <https://doi.org/10.1016/j.jmapro.2014.05.003>
21. Wu X, Li L, He N, Yao C, Zhao M (2016) Influence of the cutting edge radius and the material grain size on the cutting force in micro cutting. *Precis Eng* 45:359–364. <https://doi.org/10.1016/j.precisioneng.2016.03.012>
22. Biermann D, Steiner M (2012) Analysis of micro burr formation in austenitic stainless steel x5crni18-10. *Procedia CIRP* 3:97–102. <https://doi.org/10.1016/j.procir.2012.07.018>. (45th CIRP Conference on Manufacturing Systems 2012)
23. Weule H, Hntrup V, Tritschler H (2001) Micro-cutting of steel to meet new requirements in miniaturization. *CIRP Ann* 50(1):61–64. [https://doi.org/10.1016/S0007-8506\(07\)62071-X](https://doi.org/10.1016/S0007-8506(07)62071-X)
24. Pratap T, Patra K, Dyakonov AA (2015) Modeling cutting force in micromilling of ti-6al-4v titanium alloy. *Proc Eng* 129:134–139. <https://doi.org/10.1016/j.proeng.2015.12.021>. (International Conference on Industrial Engineering (ICIE-2015))
25. Yun HT, Heo S, Lee MK, Min B-K, Lee SJ (2011) Ploughing detection in micromilling processes using the cutting force signal. *Int J Mach Tools Manuf* 51(5):377–382. <https://doi.org/10.1016/j.ijmactools.2011.01.003>
26. Bal'azs BZ, Geier N, Tak'acs M, Davim JP (2021) A review on micromilling: recent advances and future trends. *Int J Adv Manuf Technol* 112(3):655–684. <https://doi.org/10.1007/s00170-020-06445-w>
27. Gao Q, Guo G-Y, Cai M (2021) Wear mechanism and experimental study of a tool used for micro-milling single-crystal nickel-based superalloys. *Int J Adv Manuf Technol* 113:117–129
28. Ziberov M, da Silva MB, Jackson M, Hung WNP (2016) Effect of cutting fluid on micromilling of ti-6al-4v titanium alloy. *Proc Manuf* 5:332–347. <https://doi.org/10.1016/j.promfg.2016.08.029>. (44th North American Manufacturing Research Conference, NAMRC 44, June 27–July 1, 2016, Blacksburg, Virginia, United States)
29. Torkamani H, Raygan S, Rassizadehghani J (2014) Comparing microstructure and mechanical properties of aisi d2 steel after bright hardening and oil quenching. *Mater Des* 1980–2015(54):1049–1055. <https://doi.org/10.1016/j.matdes.2013.09.043>
30. Roberts G, Krauss G, Kennedy R (1998) *Tool Steels*, 5th edn. ASM International, Ohio. <https://doi.org/10.31399/asm.tb.ts5.9781627083584>
31. Son SM, Lim HS, Ahn JH (2005) Effects of the friction coefficient on the minimum cutting thickness in micro cutting. *Int J Mach Tools Manuf* 45(4):529–535. <https://doi.org/10.1016/j.ijmactools.2004.09.001>
32. G99–05 A (2010) Standard test method for wear testing with a pin-on-disk apparatus. *Am Soc Testing Mater* 1–6. <https://doi.org/10.1520/G0099-17>
33. Zel T (2006) The influence of friction models on finite element simulations of machining. *Int J Mach Tools Manuf* 46(5):518–530. <https://doi.org/10.1016/j.ijmactools.2005.07.001>
34. Câmara MA, Abrão AM, Rubio JCC, Godoy GCD, Cordeiro BS (2016) Determination of the critical undeformed chip thickness in micromilling by means of the acoustic emission signal. *Precis Eng* 46:377–382. <https://doi.org/10.1016/j.precisioneng.2016.06.007>
35. Blau PJ (2008) *Friction Science and Technology: from Concepts to Applications*. CRC Press
36. Malayath G, Sidpara AM, Deb S (2020) Study of different materials response in micro milling using four edged micro end mill tools. *J Manuf Process* 56:169–179. <https://doi.org/10.1016/j.jmapro.2020.04.079>
37. Medeossi F, Sorgato M, Bruschi S, Savio E (2018) Novel method for burrs quantitative evaluation in micro-milling. *Precis Eng* 54:379–387. <https://doi.org/10.1016/j.precisioneng.2018.07.007>
38. Hajiahmadi S (2019) Burr size investigation in micro milling of stainless steel 316l. *Int J Light Mater Manuf* 2(4):296–304. <https://doi.org/10.1016/j.ijlmm.2019.07.004>. (Research progress on subtractive and additive manufacturing)
39. Piquard R, Dacunto A, Laheurte P, Dudzinski D (2014) Micro-end milling of niti biomedical alloys, burr formation and phase transformation. *Precision Engineering* 38(2):356–364. <https://doi.org/10.1016/j.precisioneng.2013.11.006>
40. Uzun I, Aslantas K, Bedir F (2015) Technical note. *Precis Eng* 41(1):135–144. <https://doi.org/10.1016/j.precisioneng.2015.01.002>
41. Gao S, Pang S, Jiao L, Yan P, Luo Z, Yi J, Wang X (2017) Research on specific cutting energy and parameter optimization in micro-milling of heat-resistant stainless steel. *Int J Adv Manuf Technol* 89(1–4):191–205. <https://doi.org/10.1007/s00170-016-9062-x>
42. Filiz S, Conley CM, Wasserman MB, Ozdoganlar OB (2007) An experimental investigation of micro-machinability of copper 101 using tungsten carbide micro-endmills. *Int J Mach Tools Manuf* 47(7):1088–1100. <https://doi.org/10.1016/j.ijmactools.2006.09.024>
43. Aramcharoen A, Mativenga PT (2009) Size effect and tool geometry in micromilling of tool steel. *Precis Eng* 33(4):402–407. <https://doi.org/10.1016/j.precisioneng.2008.11.002>
44. Mathai G, Melkote S, Rosen D (2012) Effect of machining parameters on burr size of micromilled foils. In: *Proceedings of the 7th International Conference on MicroManufacturing*, pp. 11–14
45. Wu Y, Chen N, Bian R, He N, Li Z, Li L (2020) Investigations on burr formation mechanisms in micro milling of high-aspect-ratio titanium alloy ti-6al-4v structures. *Int J Mech Sci* 185:105884. <https://doi.org/10.1016/j.ijmecsci.2020.105884>
46. Mhamdi MB, Salem SB, Boujelbene M, Bayraktar E (2013) Experimental study of the chip morphology in turning hardened aisi d2 steel. *J Mech Sci Technol* 27:3451–3461

Publisher's note Springer Nature remains neutral with regard to jurisdictional claims in published maps and institutional affiliations.

Springer Nature or its licensor (e.g. a society or other partner) holds exclusive rights to this article under a publishing agreement with the author(s) or other rightsholder(s); author self-archiving of the accepted manuscript version of this article is solely governed by the terms of such publishing agreement and applicable law.